# The influence of skew supports on the behaviour of multibox bridges

Autor(en): **Billington, C.J. / Dowling, P.J.**

Objekttyp: **Article**

Zeitschrift: **IABSE publications = Mémoires AIPC = IVBH Abhandlungen**

Band (Jahr): **36 (1976)**

PDF erstellt am: **23.09.2024**

Persistenter Link: https://doi.org/10.5169/seals-911

# The Influence of Skew Supports on the Behaviour of Multibox Bridges

*L'influence d'appuis biais sur le comportement de ponts à caissons multiples*

*Einfluss schiefer Auflager auf das Verhalten mehrzelliger Kastenträgerbrücken*

C.J. BILLINGTON
Head of Structures Section, Wimpey Laboratories, London

P.J. DOWLING
Reader in Steel Structures, Imperial College, London

## 1. Introduction

The layout of modern motorway and urban highway grade separated interchanges often necessitates the use of skew supports for the elevated structures. The particular advantages of the box section over other forms of construction in such situations stem from the high torsional stiffness of the closed section which ensures good transverse distribution of eccentric forces. Skew supports introduce higher torsional moments into the box girders than occur in the equivalent right supported bridge and the effects caused by distortion of the cross-section are correspondingly more pronounced. In this paper the behaviour of skew supported multibox girder bridges is illustrated by reference to theoretical and model analyses of a skew supported composite twin box structure.

The model test demonstrates the applicability of a finite element (FE) computer program to this form of construction and also establishes quickly and cheaply the critical loading positions. The FE program is then used to study the behaviour of the twin box structure with particular emphasis on the efficiency of alternative diaphragming systems to restrict the effects of distortion of the cross-section.

## 2. Description of the Model Structure

The overall dimensions of the structure are typical of motorway slip road structures in multilevel interchanges where the layout of the carriageways often necessitates a high degree of skew. The model represents to a scale of 1:30 part of a continuous structure and consists of a single simply supported span of approximately 35 m (116.7 ft).

The exact model dimensions are shown in Fig. 1. The model scale of 1/30 of full-scale was the most suitable for the available materials and laboratory testing apparatus.

The steel boxes were each manufactured from a single sheet of Birmingham Gauge 24 (0.02476 in, 0.629 mm) mild steel which was folded around a specially

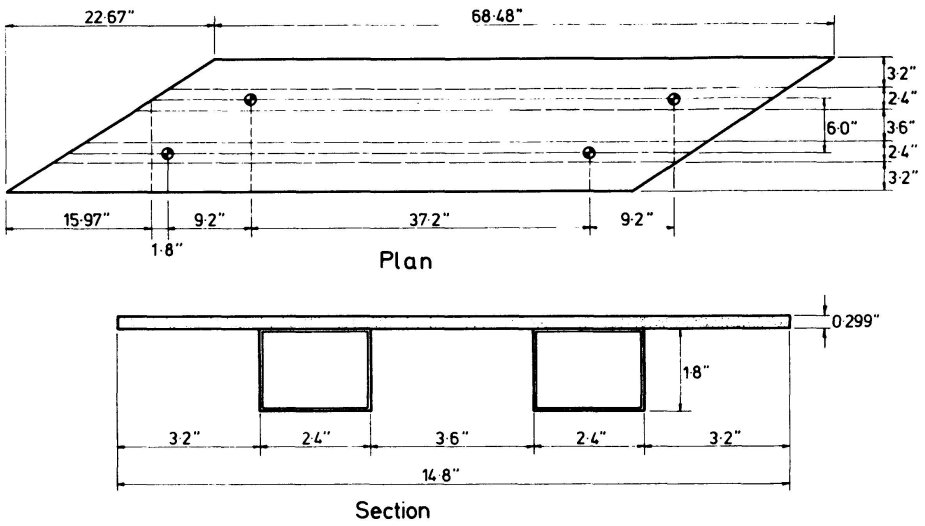


Fig. 1. Model Dimensions.

prepared former to produce the box section. The boxes were formed so that there was a longitudinal joint along the centre-line of the bottom flange. At this location the distortional warping stresses and transverse distortional bending stresses are both theoretically zero and only shear forces and transverse in-plane forces (in general low) act across the joint. An adhesive with a high shear strength was used to bond 25 mm (1 in) wide strips of .127 mm (0.005 in) thick steel both inside and outside the bottom flange to complete the joint. The strips gave sufficient area to provide the shear connection but added very little to the total inertia of the cross-section.

The model slab was made from an Araldite CY219 casting resin and sand mixture which has elastic properties very similar to those of concrete. The slab was cast in a steel mould and, after curing, the boxes were bonded to the under surface of the slab with an epoxy adhesive. The completed model is shown in Fig. 2, and the elastic properties of the model materials measured by tensile tests are given in Table 1.

*Table 1. Elastic properties of model materials*

| Material | E (Young's Modulus) | | t (thickness) | | ν (Poisson's Ratio) |
|---|---|---|---|---|---|
| | N/mm$^2$ | lbf/in$^2$ | mm | in | |
| Steel | $19.3 \times 10^4$ | $28 \times 10^6$ | 0.629 | 0.0248 | 0.3 |
| Araldite and Sand | $1.64 \times 10^4$ | $2.38 \times 10^6$ | 7.59 | 0.299 | 0.227 |

Single bearings which allow both rotation and translation were located centrally beneath each box at the pier positions. The bearings consisted of 12 mm (½ in) diameter .79 mm (1/32 in) thick rubber pads mounted on columns instrumented to measure the support reactions. The columns were located on a heavy steel *I*-section girder which was supported about .9 m (3 ft) above the laboratory floor. The moving loading frame also rested on the *I*-section with the load hanging beneath from the frame. The general testing arrangement is shown in Fig. 3. The loading system simulated a British Standard abnormal heavy vehicle (Type HB

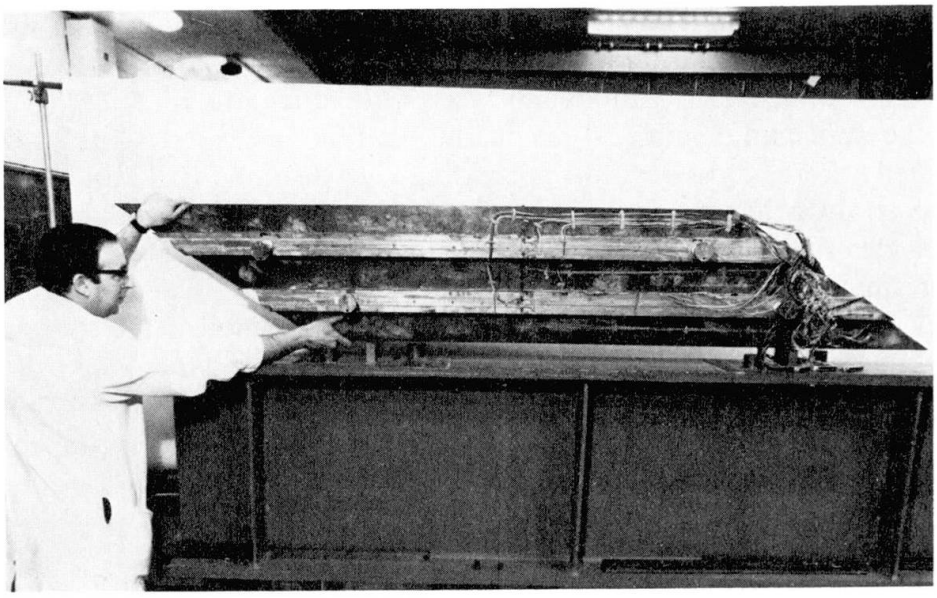

Fig. 2. Underside of Instrumented Model.

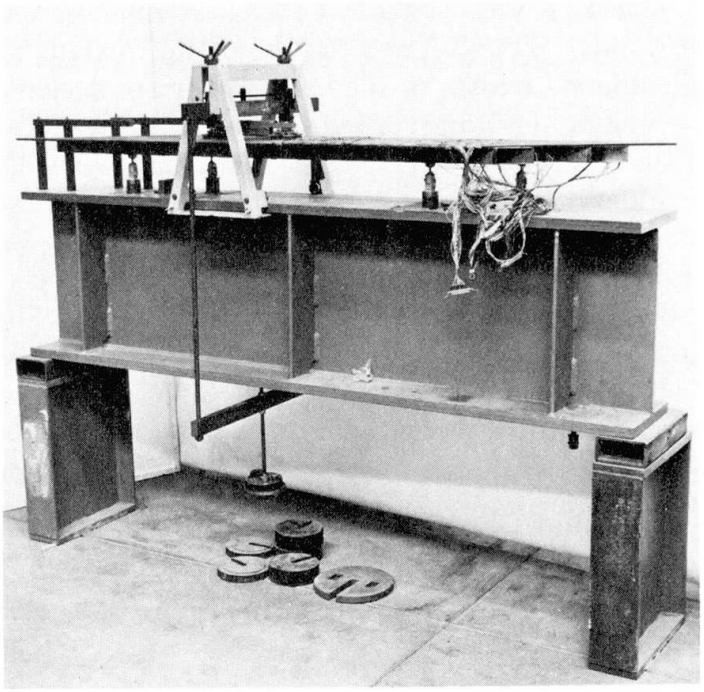

Fig. 3. Model in Test Rig.

loading) [1] of the correct scale, and the load was chosen in the correct proportion to give the same stresses in the model as would occur in the equivalent full-scale structure so that the results would be directly meaningful. Thus for the correct stresses the bending moment scale was 1:27000 and the shear force scale was 1:900. The concentrated load scale was 1:900 and the distributed load scale 1:30 for the same unit length. One HB wheel load of 112 kN (11.25 tonf) was represented by a model load of 124.5 N (28 lbf) and 45 units of HB loading 1793 kN (180 tonf) was represented by 1993 N (448 lbf).

Strains, deflections and reactions were measured experimentally. The strains were measured in both the longitudinal and transverse directions by electrical resistance strain gauges bonded to the model surfaces. Gauge lengths of 3 mm (.12 in) were used on the steel and 5 mm (.20 in) on the Araldite and sand slab. Strain gauges were located at three cross-sections coinciding with Sections 10, 12 and 14 of the FE mesh. The strain gauge readings were processed to give stresses in the longitudinal and transverse directions. Vertical and horizontal deflections were measured with dial gauges having a resolution of .0025 mm (0.0001 in). Sufficient deflections were measured at Sections 10 and 14 to define the movements of the four corners of each box so that the distorted shape of the cross-section could be determined. Vertical deflections of the model were also measured above the support positions so that the settlement of the rubber bearings could be allowed for in the comparison of theoretical and experimental results.

## 3. Description of the Finite Element Analysis

The Imperial College Structural Analysis System (ICSAS) [2] was used to analyse the model. The mesh selected for the analysis consisted mainly of rectangular elements with triangular elements used only where the geometry made this necessary at the ends of the model. The stiffness matrix of the rectangular elements is a combination of the stiffness matrix of the standard flexural element [3] and that of a plane stress element developed specially for box girder analysis [4]. The stiffness matrix of the triangular elements is a combination of the stiffness matrix of the standard flexural element [5] and that of the standard plane stress element [3].

Figure 4 illustrates the mesh used in the analysis. The longitudinal mesh lines are the minimum required to define the geometry of the cross-section and the support positions. Analytical tests on a single cell box [6] suggested that satisfactory accuracy would be obtained with this layout. These tests also indicated that only 10 web elements were necessary along the span.

The composite plates which formed the top flanges of the box girders were represented by equivalent homogeneous plates for which the appropriate value of Poisson's ration $\nu_{eff}$ was given by:

$$\nu_{eff} = \sqrt{\nu_{steel} \times \nu_{concrete}}$$

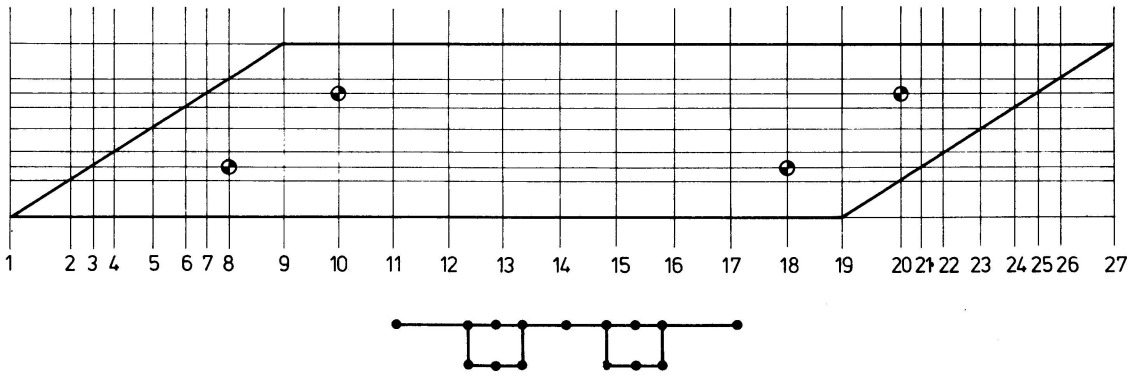


Fig. 4. Finite Element Mesh.

and the thickness $t_{eff}$ and Young's Modulus $E_{eff}$ were then calculated from the simultaneous equations:

$$\frac{E_{eff}\, t_{eff}^{3}}{12\,(1-\nu_{eff}^{2})} = D_{composite}$$

and

$$\frac{E_{eff}\, t_{eff}}{(1-\nu_{eff}^{2})} = C_{composite}$$

where $D_{composite}$ and $C_{composite}$ are the flexural and extensional rigidities of the composite plate. The elastic properties of the top flange plate used in the analysis were:

$$\nu_{eff} = 0.261,\ t_{eff} = 9.04 \text{ mm } (0.356 \text{ in}),\ E_{eff} = 2.72 \times 10^{4} \text{ N/mm}^2\ (3.95 \times 10^{6} \text{ lbf/in}^2)$$

## 4. Comparison of Model and Finite Element Results

Three loading cases were used in the comparison and their positions are shown in Fig. 5. Load case 1 was chosen to give high transverse distortional stresses near the centre of the span and high longitudinal stresses in the steel box under the load. Load case 2 was chosen to give high transverse bending stresses in the slab opposite one of the inner supports where the differential deflection between the two boxes will be high, and to give high distortional stresses in the loaded box. Load case 3 was chosen to give high transverse bending stresses in the slab at centre span. The load used in the comparison was the scale *HB* load of 1993 *N* (448 lbf).

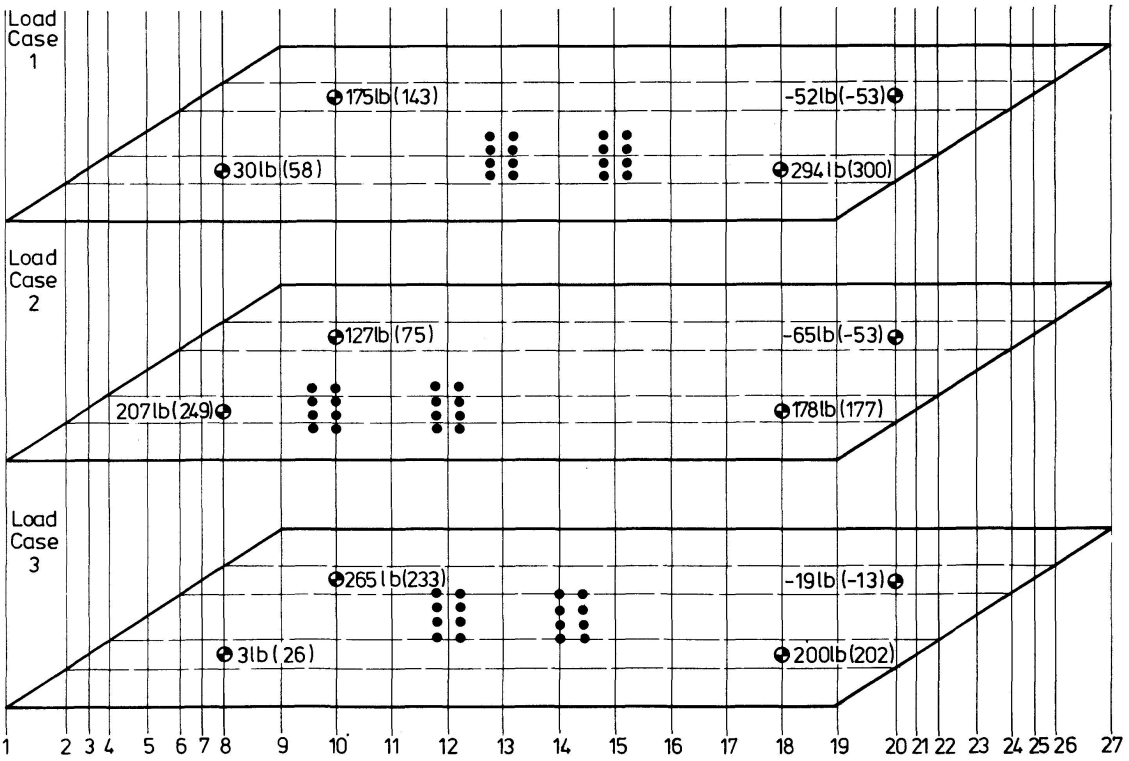


Fig. 5. Positions of 448 lb HB Vehicle for Load Cases 1-3. The F.E. Support Reactions are Shown together with the Model Reactions which are in Parentheses.

Model and *FE* deflections are plotted in Fig. 6. The model and *FE* vertical deflections show good agreement with the *FE* results slightly underestimating those of the model (maximum deflection by 2%) indicating that longitudinal stresses and transverse slab stresses should also agree closely. The agreement of transverse deflections is not quite as good indicating that there may be larger discrepancies in the comparison of transverse distortional bending stresses.

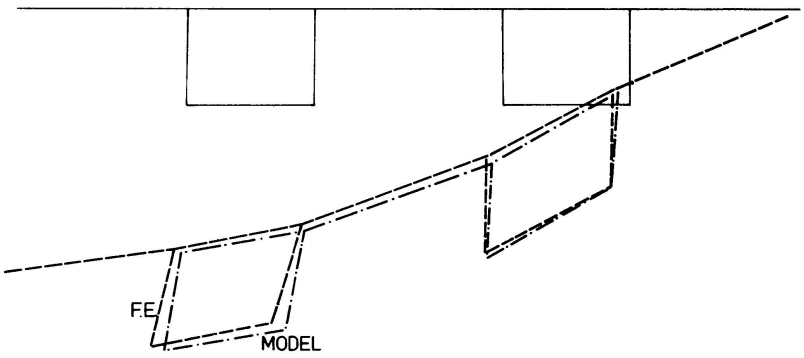


Fig. 6a. Model and F.E. Deflections at Section 14 for Load Case 1.

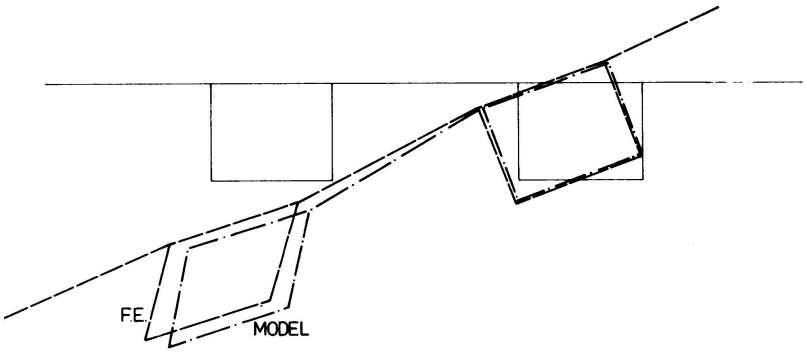


Fig. 6b. Model and F.E. Deflections at Section 14 for Load Case 3.

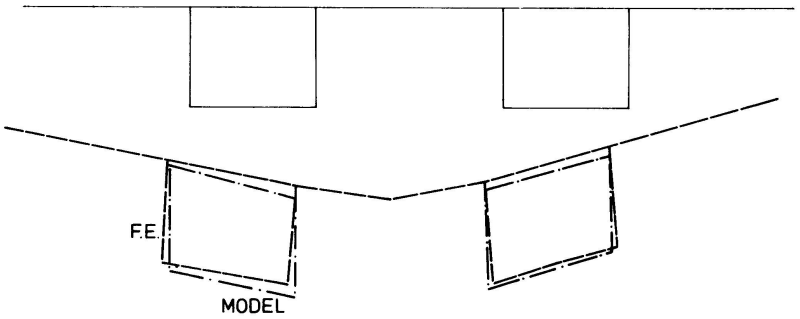


Fig. 6c. Model and F.E. Deflections at Section 14 for Load Case 3.

Typical model and finite element stress results are shown in Fig. 7. There was good agreement between the longitudinal stresses measured in the model, both for the steel and Araldite and sand, and those given by the finite element analysis. The maximum longitudinal steel stress measured in the model was for Load case 1 at Section 14 where a stress of 89 N/mm$^2$ (12911 lbf/in$^2$) was obtained (Fig. 7*a*). The maximum longitudinal slab stress at this section was 4.04 N/mm$^2$ (586 lbf/in$^2$). The maximum transverse distortional stresses in the steel boxes at Section 12 were accurately predicted by the *FE* analysis (Fig. 7*b*) but the agreement

was less good for some of the smaller distortional stresses elsewhere. There was generally good correlation for the transverse slab stresses. The maximum occurred at Section 14 in the centre of the slab for Load case 3 (Fig. 7*c*). The maximum stress is lower in the model than that given by the *FE* analysis and generally the *FE* results slightly overestimate the high slab stresses.

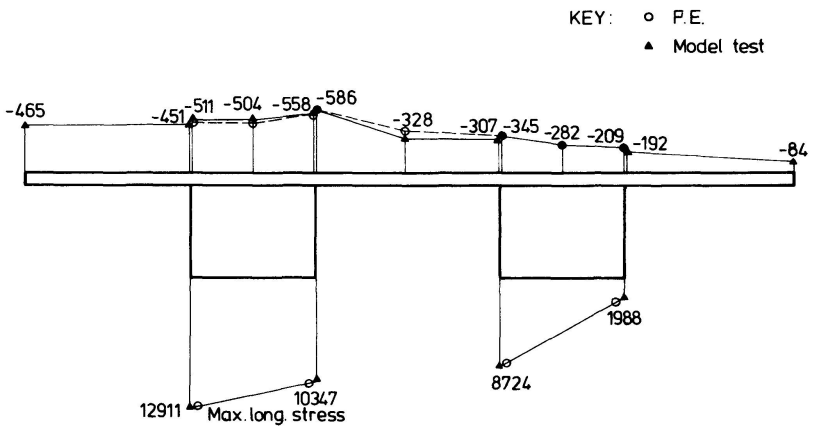


Fig. 7a. Longitudinal Stresses at Section 14 for Load Case 1.

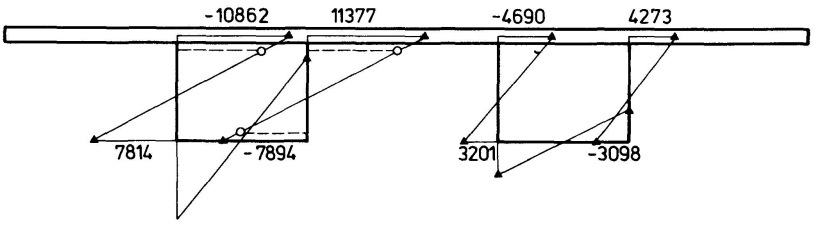


Fig. 7b. Flexural Component of the Transverse Steel Stresses at Section 12 for Load Case 2.

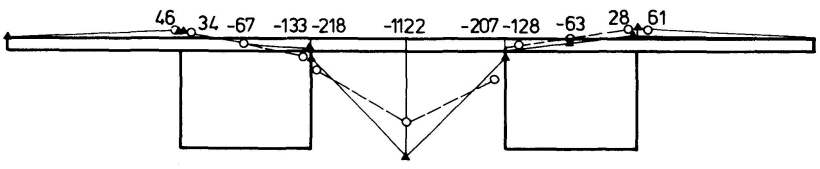


Fig. 7c. Transverse Stresses at Section 14 for Load Case 3.

A more extensive comparison of model and *FE* results is presented in Reference 7. The generally good agreement between the model results and the *FE* analysis verifies the applicability of the *FE* approach to this type of structure and shows that the mesh is sufficiently fine for the satisfactory calculation of transverse distortional stresses and transverse slab stresses.

## 5. The Structural Behaviour of the Undiaphragmed Model

Finite element results for the three loading cases of Fig. 5 were used to study the structural behaviour of the undiaphragmed model. *FE* deflections and flexural components of transverse stresses for the three loading cases are plotted in Figs 8 to 10 and 11 to 13 respectively. It was found to be useful to superimpose the deflections at several cross-sections for any particular loading case so that the influence of the skew supports on the response of the complete structure can be seen more clearly.

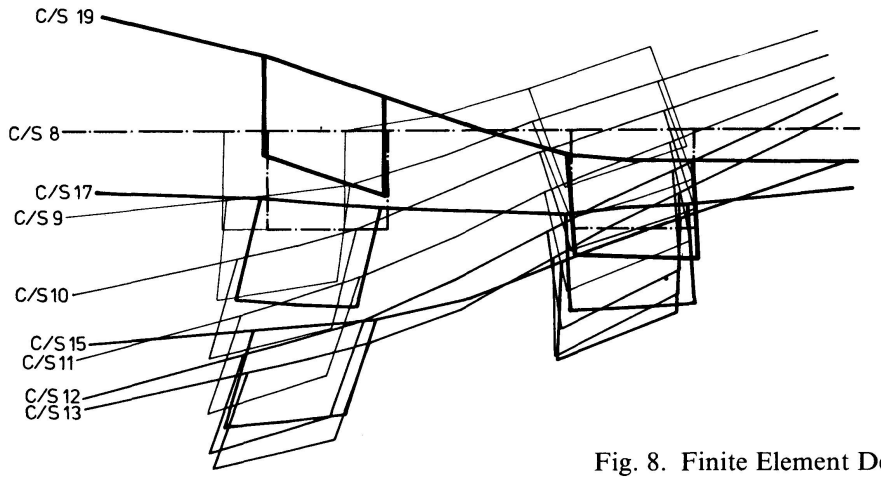


Fig. 8. Finite Element Deflections for Load Case 1.

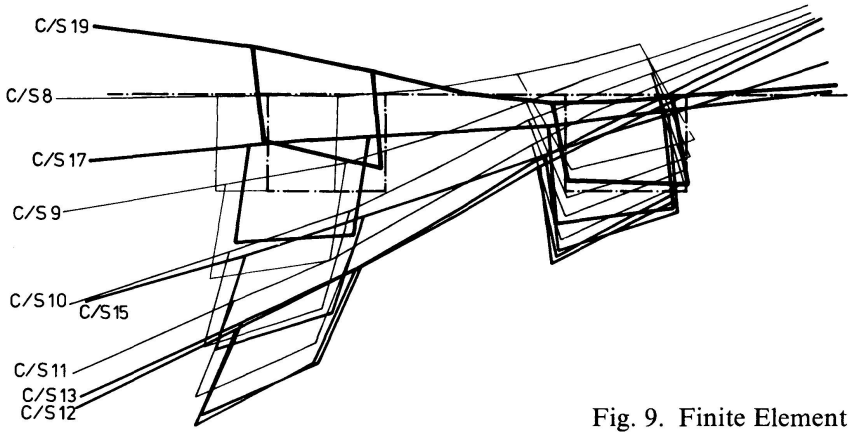


Fig. 9. Finite Element Deflections for Load Case 2.

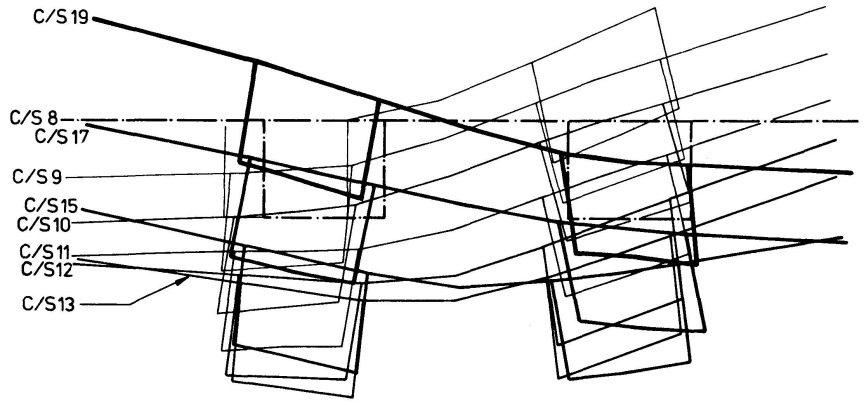


Fig. 10. Finite Element Deflections for Load Case 3.

The support diaphragms prevent distortion of the box girders above the piers but the central bearing does not provide a torsional restraint. The torsional resistance is provided by the flexural stiffness of the slab spanning between the box girder supports. Maximum vertical deflections occur under the outer web of the loaded box at Section 13 for Load cases 1 and 2.

Considering the Load case 1 results, and progressing along the loaded box from the support diaphragm at Section 8, the deformations and distortional stresses increase rapidly away from the support. The maximum transverse distortional stress 56.09 N/mm$^2$ (8135 lbf/in$^2$) occurs at Section 12 (Fig. 11, Point A). There is a high differential deflection between the inner webs of the two boxes opposite the inner support which reduces towards mid-span as the support at Section 18 is approached until, at Section 18, the distortions and deflections occur in the unloaded box only. The transverse slab stresses are high near the supports (Fig. 11, Point B), where the differential deflection is large, and locally under the axles of the *HB* vehicle (Fig. 11, Point C). The large differential deflection and rotation at the diaphragmed inner support result in an upward deflection of the unloaded cantilever.

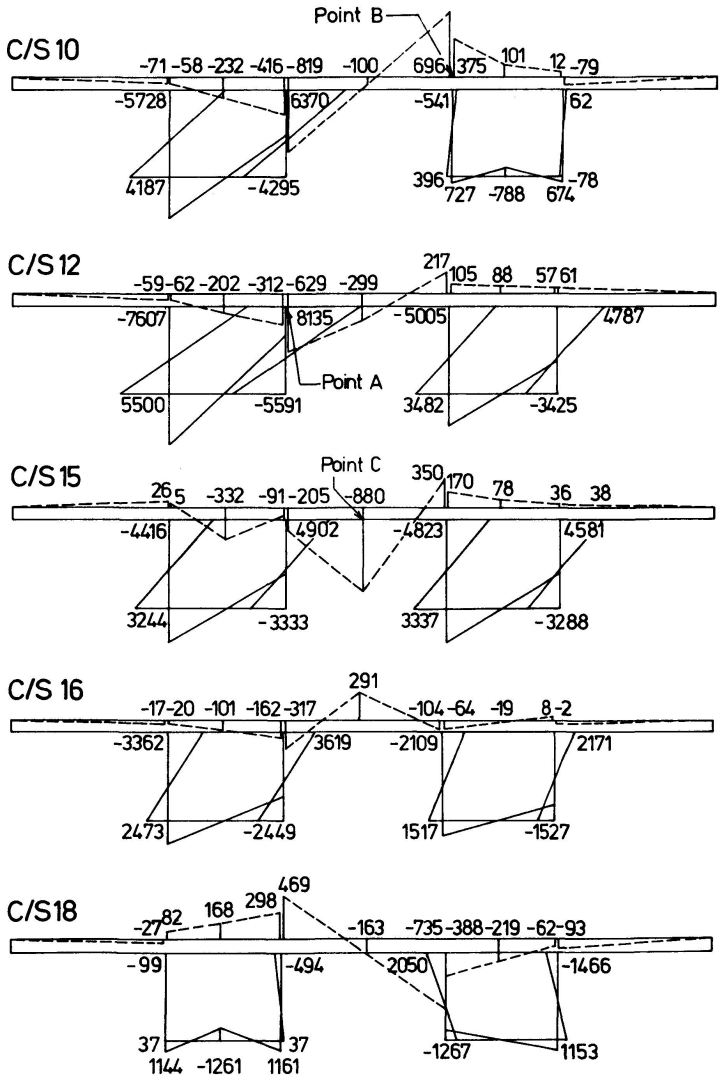


Fig. 11. Finite Element Transverse Stresses for Load Case 1.

The results for Load case 2 may be studied in a similar way. The differential deflections between the boxes opposite the inner support at Section 10 are now greater because the *HB* vehicle is opposite the support and at the position of maximum eccentricity. The rotation of the diaphragm, the upward deflection of the cantilever and the distortional stresses in the loaded box are also increased. The maximum transverse distortional stress 78.44 N/mm$^2$ (11377 lbf/in$^2$) occurs at Section 12 (Fig. 12, Point D). Because of the high differential deflection, the maximum transverse slab stress is also larger and occurs where the slab joins the inner edge of the box at the diaphragm (Fig. 12, Point E). The diaphragm prevents the relief of the slab stresses which occurs elsewhere where the distortion of the box reduces the otherwise rapid change of curvature in the slab at the edge of the box.

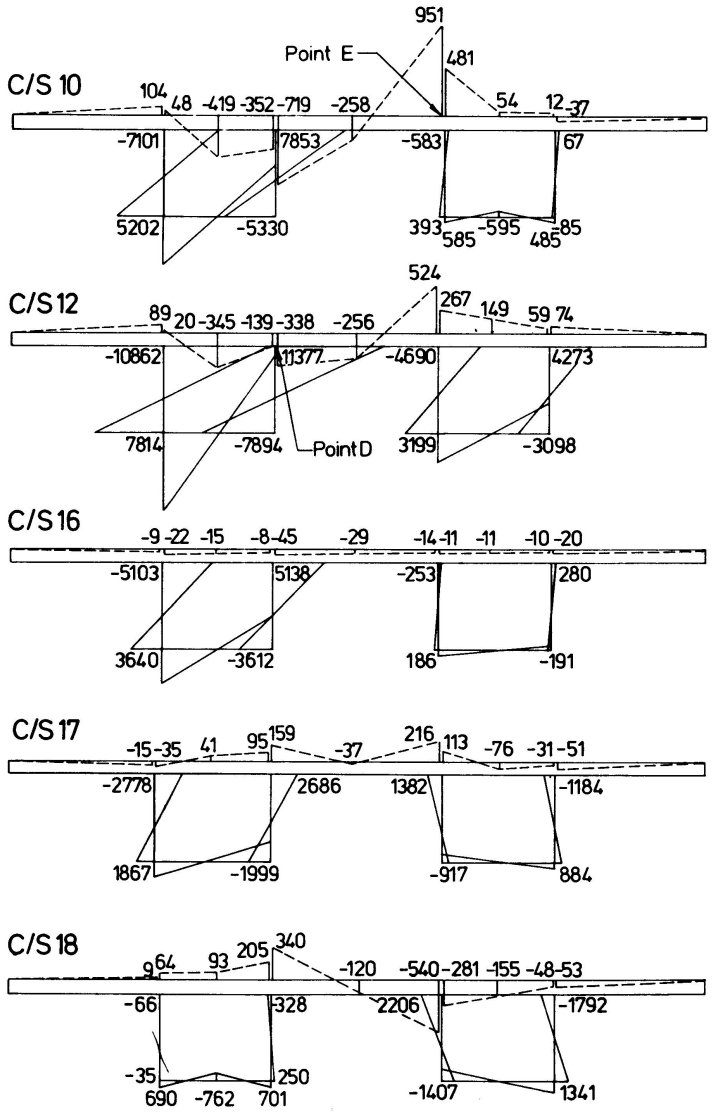


Fig. 12. Finite Element transverse Stresses for Load Case 2.

For Load case 3 the deflected shape is quite different and the differential deflections between the two boxes are low. The distortional stresses in the boxes are also low 28.17 N/mm$^2$ (4086 lbf/in$^2$ maximum Fig. 13, Point F), but the maximum distortions still occur near the inner supports at Sections 10 and 18. The upper

surface of the slab is concave between the boxes and the structure tends to span between the inner supports with small uplift forces at the outer supports. The maximum transverse slab stresses occur at Section 14 (Fig. 13, Point G) under one of the axles of the *HB* vehicle.

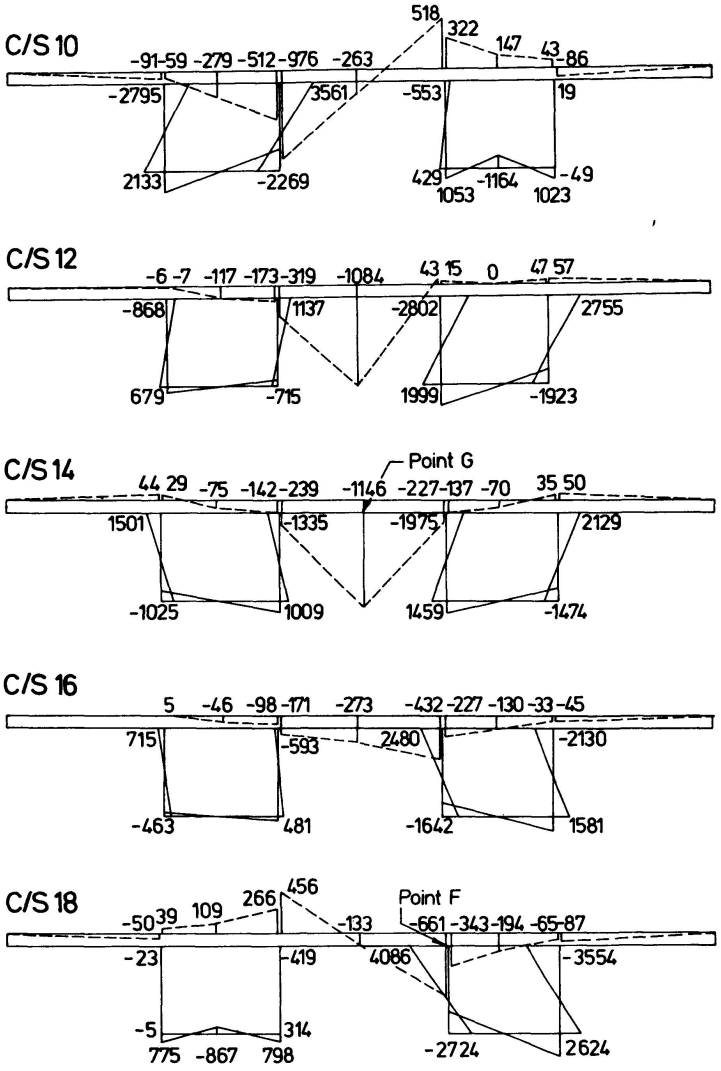


Fig. 13. Finite Element transverse Stresses for Load Case 3.

The results of all three loading cases show how the inner supports act as eccentric loads on the unsupported box producing large distortions of the cross-section and correspondingly large transverse bending stresses opposite the inner supports.

The magnitudes of the steel stresses are not high and their full significance is only realised when the full-scale transverse moments, calculated from model stresses, are applied to a typical full-scale combined stiffener and effective width of plate section of the prototype structure. For the maximum model stress 78.44 N/mm$^2$ (11377 lbf/in$^2$) the equivalent full-scale stress would approach yield stress which is clearly unacceptable. Longitudinal stresses and transverse slab stresses are directly applicable to full-scale behaviour and with suitable steel reinforcement in the slab they could be readily catered for in the design.

## 6. A Study of Various Diaphragming Arrangements for the Skew Supported Model

The analysis of the undiaphragmed model described in Section 5 showed that transverse distortional bending stresses reached unacceptable levels under working loads. Therefore a study was carried out using the *FE* program to evaluate the effects of different diaphragm layouts on the transverse distortional stresses in the box girders and the transverse stresses in the slab. The various diaphragm configurations considered are shown in Fig. 14 and the results relating to these positions were also compared with the equivalent right bridge (Fig. 15), with a span of 1178 mm (46.4 in) to isolate the effects of skew on the distortional behaviour. Bar elements in the form of cross-bracing were used to simulate the diaphragms as these could be introduced into the *FE* analysis without altering the remainder of the data for the program. The bar elements were proportioned to provide the same distortional stiffness as 12 mm (½ in) plate diaphragms in the full-scale structure. The load positions used in the study were the same as those used in the original analysis of the undiaphragmed model as these were judged to approximate closely the critical positions for the various diaphragm configurations considered. The results of the study are summarised in Figs 16 to 18 which show the maximum transverse box and slab stresses for each diaphragm arrangement.

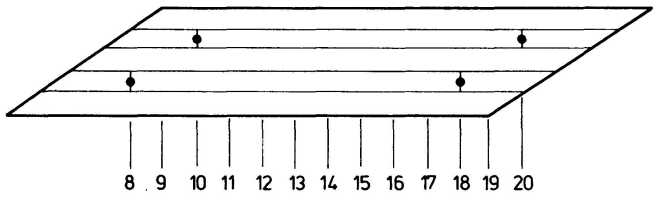


Diaphragm layout 1 - undiaphragmed model

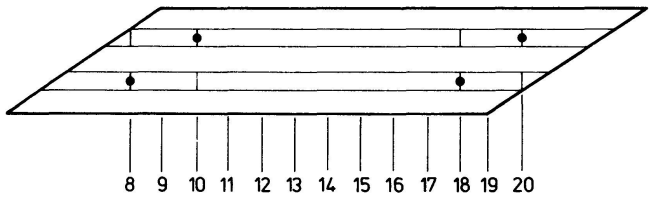


Diaphragm layout 2 - internal bracing at Sections 10 and 18

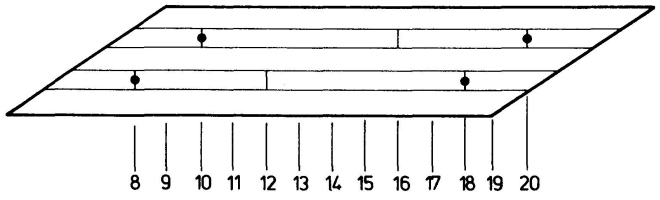


Diaphragm layout 3 - internal bracing at Sections 12 and 16

Fig. 14a. Diaphragm Layouts 1-3.

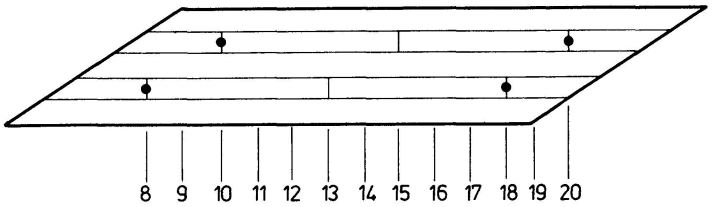


Diaphragm layout 4 - internal bracing at Sections 13 and 15

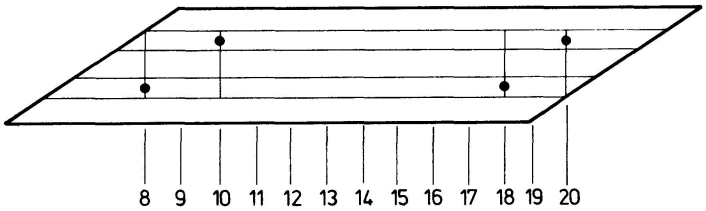


Diaphragm layout 5 - bracing in and between boxes at Sections 10 and 18

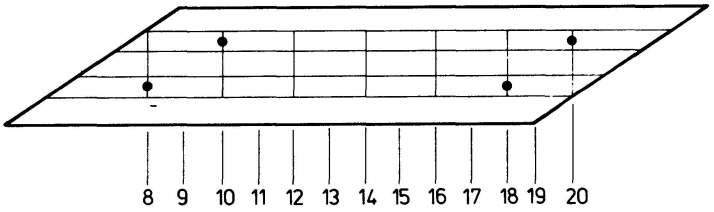


Diaphragm layout 6 - fully diaphragmed model

Fig. 14b. Diaphragm Layouts 4-6.

High transverse distortional bending stresses, $\sigma_{DB}$, occurred in the box girders opposite inner skew supports. It would appear therefore that one possible modification which would restrict these stresses would be to provide diaphragming within the box in this region. To this end, the analysis of Diaphragm Layout 2, which incorporates cross-bracing at Sections 10 and 18, was carried out. Figures 16 to 18 show that the maximum $\sigma_{DB}$ in the loaded box is reduced from 78.44 N/mm$^2$ (11,377 lbf/in$^2$) for Load case 2 at Section 12 to 40.16 N/mm$^2$ (5,824 lbf/in$^2$) for Load case 2 at Section 13 and the maximum $\sigma_{DB}$ in the unloaded box is almost unchanged 44.92 N/mm$^2$ (6,515 lbf/in$^2$) for the undiaphragmed case to 42.42 N/mm$^2$ (6,152 lbf/in$^2$) — both for Load case 1 at Section 13. However, the maximum transverse slab stress at Section 10 for Load case 2 is increased from 6.56 N/mm$^2$ (951 lbf/in$^2$) to 10.42 N/mm$^2$ (1,511 lbf/in$^2$) and the latter value would be unacceptable at full-scale. The undiaphragmed box, due to its lack of distortional stiffness, can more readily follow the transverse deflected shape of the slab and therefore transverse moments are lower than those obtained when the distortion is prevented and a hard point is produced at the intersection of the edge of the box and slab. There are two possible solutions to this problem. One is to remove the hard spot by moving the diaphragm in the loaded box away from the support so that there are not two diaphragms at the same section. The distortion is then

resisted elsewhere and some distortion is allowed at the support section so that a compromise is obtained between the maximum box and slab stresses. The other solution is to prevent differential deflection of the two boxes at the support section by providing diaphragms between the boxes at these points and the transverse slab moments are then reduced to negligible proportions at that section. The latter solution has the disadvantage that the diaphragms interfere aesthetically with the clean lines of the underside of the structure.

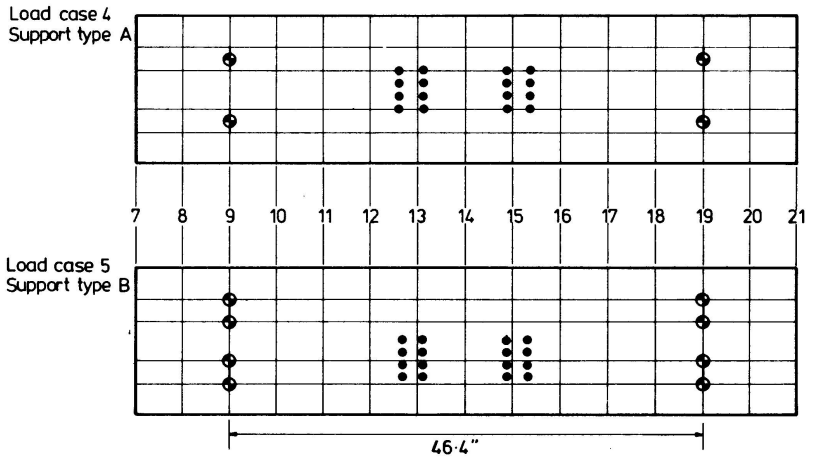


Fig. 15. Equivalent right Bridge Structures showing loading Positions 4 and 5 and alternative Support Arrangements. The section numbers have been chosen to coincide as far as possible with those of the skew structure.

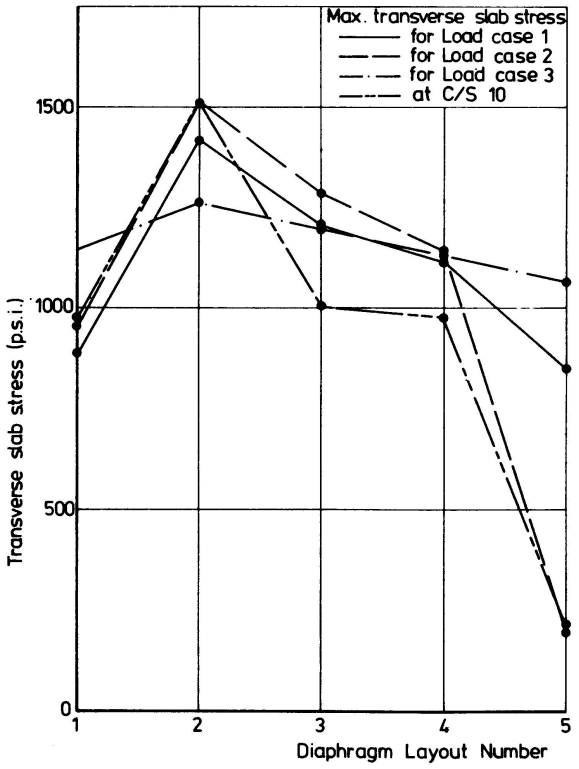


Fig. 16. Summary of Max. Transverse Slab Stresses for Diaphragm Layouts 1-5.

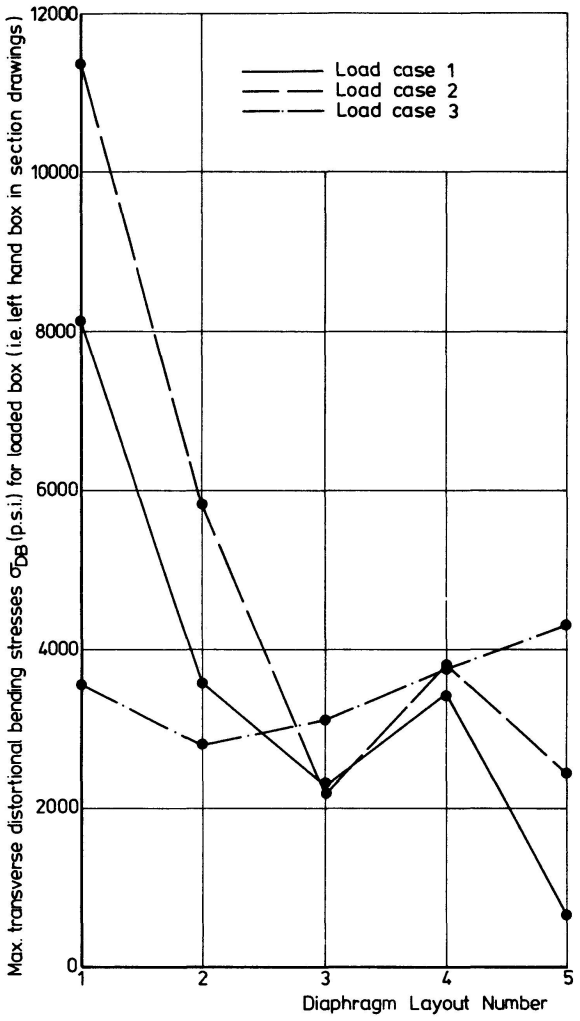


Fig. 17. Summary of Max. Transverse Distortional stresses $\sigma_{DB}$ in Loaded Box for Diaphragm Layouts 1-5.

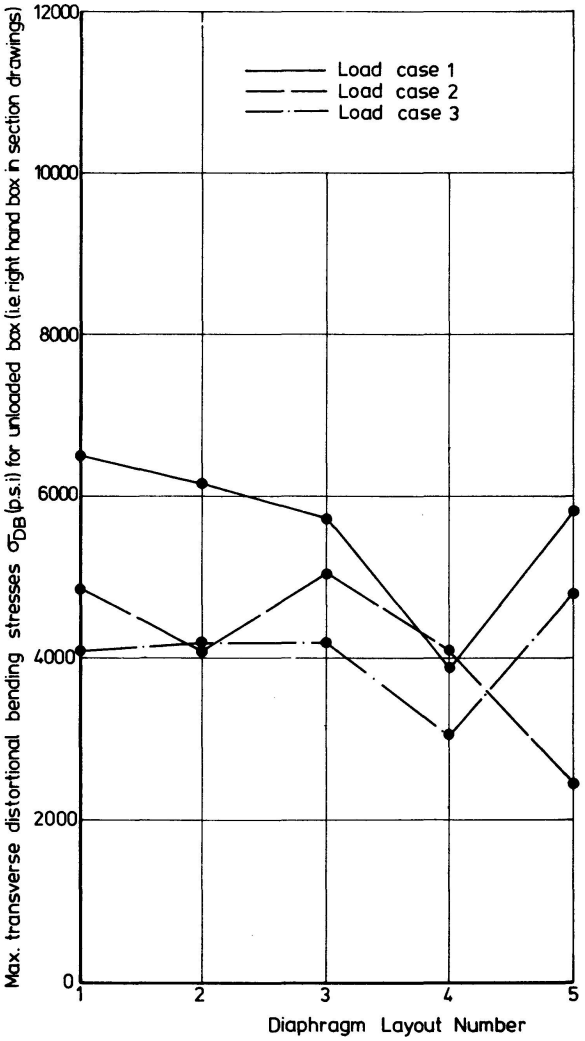


Fig. 18. Summary of Max. Transverse distortional Stresses $\sigma_{DB}$ in Unloaded Box for Diaphragm Layouts 1-5.

Both possible solutions were investigated with the *FE* program. Diaphragm Layouts 3 and 4 were analysed in order to study the effects of moving the diaphragms away from the support sections and Diaphragm Layout 5 simulates diaphragming between the box girders at support sections.

The results for Diaphragm Layouts 2, 3 and 4 are summarised in Figs 16 to 18 and show how the transverse slab stresses at Section 10 decrease as the diaphragm is moved away from the support region. The maximum transverse slab stresses occur near the diaphragms 8.98 N/mm$^2$ (1,285 lbf/in$^2$) at Section 11 for Layout 3, 7.96 N/mm$^2$ (1,140 lbf/in$^2$) at Section 13 for Layout 4 — both for Load case 2, c.f. 10.55 N/mm$^2$ (1,511 lbf/in$^2$) for Layout 2. The maximum $\sigma_{DB}$ in both boxes are also reduced as the distortional spans decrease.

The results for Diaphragm Layout 5 (bracing in and between the boxes at support sections) have also been incorporated into Figs 16 to 18. They show that although there is a considerable reduction in the transverse slab stresses at the support section, the maximum transverse slab stress for Load case 3 (7.46 N/mm$^2$ (1,068 lbf/in$^2$) at Section 14) is only marginally below that of other diaphragm layouts. The maximum $\sigma_{DB}$ is 40.45 N/mm$^2$ (5,791 lbf/in$^2$).

The results show that, of the diaphragm configurations considered, Layouts 4 and 5 are the best solutions, the maximum transverse slab stresses being marginally higher for Layout 4 and the maximum $\sigma_{DB}$ marginally higher for Layout 5. Diaphragm Layout 4 would appear to have the advantage in terms of cost and ease of fabrication.

Diaphragm Layout 6 is a fully diaphragmed scheme with bracing both in and between the boxes at even numbered sections (see Fig. 14). Transverse stresses in both the slab and the box girders are low. While this stiffening system would be effective in limiting both transverse slab and distortional bending stresses in the boxes to acceptable levels, the alternative solutions considered in Diaphragm Layouts 2 to 5 suggest that a similar objective may be achieved with possible savings in fabrication costs and considerable savings in maintenance costs by the omission of diaphragms between boxes.

## 7. A Comparison of the Skew Structure with a Right Supported Structure of Equal Span

An equivalent right supported structure with a span of 1178 mm (46.4 in) (Fig. 15) was analysed. The load cases were chosen to be symmetrical about mid-span so that it was only necessary to analyse a quarter of the structure (loads were applied as symmetrical and antisymmetrical components which were superimposed to obtain the results for eccentric loads). This resulted in large savings in computer time and storage. The results of Load case 4 are comparable with those of Load case 3 on the skew structures, while those of Load case 5 may be compared with Load case 1 on the skew structures. Two support systems were considered — Type A with a single support centrally below the box as for the skew structures, and Type B which has supports under both webs of each box at the pier positions. Thus the effects of resisting the torsional loading at the supports rather than by the slab spanning between the boxes could be investigated. The results of the analysis (which are included in Reference 7) show that although the transverse slab stresses

are higher for support Type A where torsion is resisted by the transverse action of the slab, for this structure the differences are only marginal [maximum slab stress for Type A — 8.13 N/mm$^2$ (1,164 lbf/in$^2$), for Type B — 7.73 N/mm$^2$ (1,106 lbf/in$^2$)]. The boxes resist the rotation of the slab and consequently attract higher stresses than if they were free to rotate. This is reflected by higher transverse slab stresses at the edge of the unloaded box for Load case 5.

It is interesting to compare the results of the analysis of Diaphragm Layout 5 (bracing at support sections in and between the boxes) with the results for the right bridge structure. The results for both structures show very similar behaviour, the main difference being the higher values of $\sigma_{DB}$ for the right bridge structure which has a longer distortional span. This suggests that distortional effects in skew structures with bracing of the type used in Layout 5 could be evaluated by analysing a right supported structure with a span equal to the distance between inner skew supports. With such a simplification the analysis could be carried out far more cheaply by approximate methods.

## 8. Conclusions

I. The finite element mesh used was sufficiently fine to describe accurately the behaviour of the undiaphragmed model.

II. The effects of the skew supports were to produce high differential deflections between the box girders of the undiaphragmed structure. Skew supports in the undiaphragmed multibox structures act as eccentric loads on adjacent boxes thus accentuating the distortional stresses in the box girders and the transverse moments in the slabs.

III. Transverse moments in the slab of the undiaphragmed structure could be catered for in the design of the reinforcement. In some places these moments can cause uplift forces on the shear connectors near the edges of the box girders.

IV. The maximum transverse distortional bending stresses, $\sigma_{DB}$, in the full-scale undiaphragmed structure would be near the yield stress of the material at working loads. These stresses can also be critical for the fatigue life of welds at the box corners as they are caused mainly by live loading and may therefore be fully reversible. It is necessary, therefore, to provide internal diaphragms or cross-bracings within the box girders to restrict the distortional stresses.

V. The introduction of internal diaphragms within the span in multibox structures increases the effective torsional rigidity of the boxes and thus improves the transverse distribution of load. Large transverse bending moments are also induced in the slab, however, and these are a maximum in the vicinity of the internal diaphragms as a localised but rapid change of curvature occurs in the transverse deflected profile at the points of intersection of the slab with the edge of the box.

VI. In the case of the modelled bridge it is possible to restrict the transverse distortional stresses to acceptable limits, without increasing the transverse slab moments, by a careful choice of internal diaphragm siting. Such a scheme leaves the space between boxes clear and as well as the aesthetic advantages other benefits include ease of fabrication and maintenance.

VII. If, in addition to the internal diaphragms, rigid diaphragms are provided in and between the box girders at skew support positions in a direction perpendicular to the span, the distortional response of the structure between support diaphragms is similar to that of the equivalent right supported structure with a span equal to the distance between inner skew supports.

VIII. The equivalent right bridge structure was analysed with both single and twin supports under each box to determine the effect of providing an individual torsional restraint for each box. The differences between the results of the two analyses were small as the torsional response was overshadowed by the distortional deflections, but they do indicate that the torsional stiffness of each box is small when compared with the torsional stiffness of the complete structure restrained by single supports under each box. The use of a single bearing at each support position simplifies pier and foundation design.

## 9. Acknowledgements

The work described in this paper was carried out as part of an investigation for the Department of the Environment, South Eastern Road Construction Unit.

The authors wish to thank Dr. J.C. Chapman, Technical Director, George Wimpey and Co. Ltd., for his helpful comments and suggestions when, as Reader in Structural Engineering at Imperial College, he supervised this project in its initial stages. They would also like to thank Professor S.R. Sparkes, latterly Head of the Engineering Structures Laboratories for the helpful way in which he accommodated the project throughout.

Thanks must go to the technician staff of the Engineering Structures Laboratories without whose experience and technical expertise the project would not have been possible.

Grateful acknowledgement is also made of Dr. K.R. Moffatt's assistance in making available and running his finite element computer system.

## 10. References

1. BS153, Part 3A: Specification for Steel Girder Bridges-Loads. British Standards Institution, London, 1958.
2. LIM, P.T.K., and MOFFATT, K.R.: A General Purpose Finite Element Program. Proc. P.T.R.C. Bridge Program Review Symposium, London, Jan. 1971.
3. ZIENKIEWICZ, O.C., and CHEUNG, Y.R.: The Finite Element Method in Structural and Continuum Mechanics, McGraw-Hill, London, 1967.
4. LIM, P.T.K., KILFORD, J.T., and MOFFATT, K.R.: Finite Element Analysis of Curved Box Girder Bridges. Proc. Developments in Bridge Design and Construction Conference, Cardiff, March 1971.
5. CHEUNG, Y.K., KING, I.P., and ZIENKIEWICZ, O.C.: Slab Bridges with Arbitrary Shape and Support Conditions: a General Method of Analysis Based on Finite Elements. Proc. I.C.E., Vol. 40, 1968, pp. 9-36.
6. LIM, P.T.K.: Elastic Analysis of Bridge Structures by the Finite Element Method. PhD Thesis, University of London, 1971.
7. BILLINGTON, C.J.: The Theoretical and Experimental Elastic Behaviour of Box Girder Bridges. PhD Thesis, University of London, 1974.

## Summary

This paper describes the behaviour of a skew supported multibox bridge. Skew supports introduce higher torsional moments and cross-section distortional effects into the box girders than occur in equivalent right supported spans. The test results of a model with diaphragms only at the pier positions are reported and a finite element analysis shows that with such an arrangement the stresses in the equivalent full-scale structure would be unacceptably high. The behaviour of the twin box structure with various internal and external diaphragming schemes is studied. It is shown how distortional stresses may be restricted to acceptable levels without having to resort to external diaphragms.

## Résumé

L'article décrit le comportement d'un pont biais à caissons multiples. Les appuis biais donnent lieu à des moments de torsion élevés et à des phénomènes de déformation dans les poutres à caisson. Les auteurs discutent les résultats d'essai sur un modèle muni uniquement de diaphragmes aux piliers; la méthode par élément fini montre qu'avec cette disposition la sollicitation de la superstructure atteindrait une valeur inadmissible. Le comportement du pont à caisson double avec diaphragmes intérieurs et extérieurs est étudié. On montre la manière par laquelle les sollicitations peuvent être limitées à un niveau acceptable sans avoir recours à des diaphragmes extérieurs.

## Zusammenfassung

Die vorliegende Arbeit beschreibt das Verhalten einer schief gelagerten mehrzelligen Kastenträgerbrücke. Schiefe Auflager führen zu höheren Torsionsmomenten und Querschnitts-Verwölbungen im Kastenträger als bei äquivalenten geradlinig unterstützten Öffnungen. Es wird über die Versuchsergebnisse an einem nur über den Pfeilern mit Querträgern versehenen Modell berichtet; eine finite Elementenuntersuchung zeigt, dass mit einer solchen Anordnung die Beanspruchung des Brückenträgers unzulässig hoch wäre. Das Verhalten der Doppelkastenbrücke mit verschiedenen äusseren und inneren Querträgern wird untersucht. Es wird gezeigt, wie die Spannungen auf ein zulässiges Mass beschränkt werden lönnen, ohne dass auf äussere Diaphragmen zurückgegriffen werden muss.

Leere Seite
Blank page
Page vide